Supplementary Information

An allosteric modulator of RNA binding targeting the N-terminal domain of TDP-43 yields neuroprotective properties

Niloufar Mollasalehi[1,2,3]‡, Liberty Francois-Moutal[1,2]‡, David D. Scott[1,2], Judith Arane Tello[1,2], Haley Williams[1,2], Brendan Mahoney[4], Jacob M. Carlson[1,2], Yue Dong[5,6], Xingli Li[7], Victor G. Miranda[1,2], Vijay Gokhale[8], Wei Wang[5,6], Sami J. Barmada[7], May Khanna[1,2]*

From the [1]Department of Pharmacology, College of Medicine, University of Arizona, Tucson, AZ 85724, USA; [2]Center of Innovation in Brain Science, Tucson, AZ 85721, USA; [3]Department of Chemistry and Biochemistry, University of Arizona, Tucson, AZ 85721-0041, USA;[4]Department of Chemistry and Biochemistry, University of California, Los Angeles (UCLA) Los Angeles, CA 90095, USA; 5Arizona Center for Drug Discovery, College of Pharmacy, University of Arizona, Tucson, AZ 85721, USA;[6]Pharmacology and Toxicology department, College of Pharmacy, University of Arizona, Tucson, AZ 85721, USA; 7Department of Neurology, University of Michigan Health System, Ann Arbor, MI 48109, USA ;[8]Bio5 Institute, University of Arizona, Tucson, AZ 85721, USA.

‡These authors contributed equally.

* To whom correspondence should be addressed: Dr. May Khanna, Department of Pharmacology, College of Medicine, University of Arizona, 1501 North Campbell Drive, P.O. Box 245050, Tucson, AZ 85724, USA Office phone: (520) 626-2147; Fax: (520) 626-2204; Email: maykhanna@email.arizona.edu

Supplementary methods

Materials. All reagents were purchased from Sigma and Fisher Scientific.

nTRD22 (logP 2.4) has not been previously reported as an aggregator as predicted by Aggregator Advisor[1]. A similar query of nTRD22 in the Zinc15 database revealed no hits to molecules containing PAINS chemotypes. Human TDP-$43_{1\text{-}260}$ and $TDP43_{102–269}$ were expressed as described in our previous studies[2,3].

Molecular Modeling. Molecular docking studies were performed using Schrodinger suite of programs, Glide virtual screening workflow. X-ray structure of the N-terminal domain of TAR DNA-binding protein 43 (TDP-43) (PDB ID: 5mdi[4]) and an average NMR structure (PDB ID: 2n4p[5]) were used for virtual screening of DIVERSet-CL, small molecule library of 50,000 compounds from ChemBridge. The top-ranked potential receptor binding sites were generated using siteMap screening for residues in N-terminal domain. Resulting docking poses were analyzed using XP G-score and the top compounds from X-ray structure, and from the NMR structure were selected for further screening.

Purification of recombinant TDP-43 N-terminal domain (NTD). TDP-$43_{1\text{-}102}$ was transformed into E. coli BL21 and then grown in LB media containing 50 $\mu g.mL^{-1}$ kanamycin at 37 °C overnight. Culture was inoculated into M9 media supplemented with uniformly labeled $^{15}NH_4Cl$ (Cambridge Isotope Laboratories). After the OD_{600} reached 0.8, 1 mM isopropyl β-D-1-galactopyranoside was used to induce protein expression at 30 °C overnight. Cells were collected by 4500 rpm centrifugation and resuspended in 40 mM Tris-HCl, pH 7.5, 500 mM NaCl, 5 mM DTT, 30 mM imidazole and EDTA-free protease inhibitor cocktail. Cell disruption was performed by two rounds of high-pressure homogenization at 12,000 PSI with a LM10 Microfluidizer (Microfluidics) and cell debris was removed by centrifugation at 34,000 rpm for 1h at 4°C. Supernatant was then loaded on a His-Trap (GE Healthcare) previously equilibrated using resuspension buffer. Protein was then eluted with a linear gradient of imidazole up to 400 mM. Eluted fractions of pure protein were dialyzed into NMR buffer (40 mM HEPES, pH 6.5, 500 mM NaCl, 4 mM DTT). Dialyzed protein was concentrated with Amicon Ultra 15 centrifugal filters (Regenerated cellulose 3,000 NMWL; Merck Millipore, Darmstadt, Germany).

Saturation Transfer Difference Nuclear Magnetic Resonance (STD-NMR). Spectroscopy for small molecule binding. 1D ^1H STD-NMR was performed exactly as previously described[3,6].

Heteronuclear Single Quantum Correlation-NMR (HSQC-NMR). NMR spectra were acquired in 40 mM HEPES pH 6.5, 500 mM NaCl, 4 mM DTT with 10% (v/v) D_2O at 100 μM protein concentrations using 5 mm Shigemi NMR tubes. NMR data were collected at 298 K on a Bruker Avance NEO 600 MHz and 800 MHz spectrometers with TCI-H&F/C/N probe. NMR processing and analysis was done using NMRpipe, NMRDraw and NMRFAM-Sparky[7]. Transverse relaxation optimized spectroscopy (TROSY) was used for all HSQC experiments.

Heteronuclear Single Quantum Correlation-NMR (HSQC-NMR) of NTD-RRM TDP-43. NTD as well as ^{15}N-labeled RRM aliquots were dialyzed against the following buffer: 40 mM HEPES, pH 6.5, 500 mM NaCl, for 3 hours in cold room before exchanging with fresh buffer and continuing dialysis overnight. All spectra were collected at 298 K on a 500 MHz Bruker Avance spectrometer equipped with TCI cryoprobe running TopSpin 1.3 software. Samples were individually shimmed and tuned, and carrier position and 90-degree pulse length were optimized for each sample. Each titration point consisted of ^1H 1-D WaterGATE (3-9-19) spectrum [td=2048, ns=32] as well as a ^{15}N-^1H 2-D BEST-TROSY [td=1024*128 , o3p=116 ppm, sw=14ppm,32ppm, d1=180 ms]. The number of scans was adjusted to account for changes in ^{15}N-labeled

RRM concentration (64, 256, 1024, 1792 for the four titration points, respectively). Data were processed in NMRPipe (PMID: 8520220) and visualized in NMRFAM-SPARKY[7].

Microscale Thermophoresis (MST). Microscale thermophoresis experiments were performed using a NanoTemper Monolith Instrument (NT.115), similarly to[3].

Amplified luminescent proximity homogeneous alpha assay (ALPHA). Amplified luminescent proximity homogeneous alpha assay (ALPHA) experiment was conducted as reported before[3]. TDP-$43_{1\text{-}260}$-His (0.75 nM) and a single concentration of biotinylated-UG_6 RNA (0.6 nM) with increasing concentration of nTRD22 were used.

Surface Plasmon Resonance (SPR). Surface plasmon resonance was performed with a Biacore 3000 instrument (GE Healthcare). NTD (TDP-$43_{1\text{-}102}$) was covalently immobilized on a CM5 chip using standard amine coupling according to the manufacturer's protocol. Once the protein was immobilized (2500 RU), there was a flow of (i) 500 nM TDP-$43_{1\text{-}260}$, (ii) 500 nM TDP-$43_{1\text{-}260}$ plus 1% DMSO (v/v) and (iii) 500 nM TDP-$43_{1\text{-}260}$ plus 200 μM nTRD22 with HBS-EP buffer upon immobilized protein. Binding of TDP-$43_{1\text{-}260}$ onto the immobilized NTD (TDP-$43_{1\text{-}102}$) was tested in varying conditions.

Ethics statement. All vertebrate animal work was approved by the Committee on the Use and Care of Animals (UCUCA) at the University of Michigan. Rats (*Rattus norvegicus*) used for primary neuron collection were housed singly in chambers equipped with environmental enrichment. Rats used for *in vivo* studies were housed with the dam until weaning at three weeks of age. Thereafter, they were housed in pairs by gender. All studies were designed to minimize animal use. Rats were cared for by the Unit for Laboratory Animal Medicine at the University of Michigan; all individuals were trained and approved in the care and long-term maintenance of rodent colonies, in accordance with the NIH-supported Guide for the Care and Use of Laboratory Animals. All personnel handling the rats and administering euthanasia were properly trained in accordance with the UM Policy for Education and Training of Animal Care and Use Personnel. Euthanasia was fully consistent with the recommendations of the Guidelines on Euthanasia of the American Veterinary Medical Association.

Cell culture and transfection. Rodent primary cortical neurons were prepared as before[8–10]. Briefly, neurons dissected from embryonic day 20-21 Long Evans rat pups were cultured at a density of 0.6×10^6 cells ml^{-1} in 96 well plates coated with laminin (Corning) and D-polylysine (Millipore). Primary neurons were transfected with plasmids 4 days after plating using Lipofectamine 2000 (Invitrogen) as described in[9]. rTRD022 or vehicle was added 24 h after transfection, immediately following the first imaging run.

Fluorescence microscopy. Primary cortical neurons were imaged using an automated microscopy platform described previously[8–10]. Briefly, images were obtained with an inverted Nikon TiE-2000 microscope equipped with a Nikon PerfectFocus 3 system, a high-numerical aperture 20x objective lens, Chroma ET Sedat filter sets, Sutter 4-2-1 multiLED system, and Andor Zyla 4.2+ sCMOS camera. Stage movements were accomplished using an ASI 2000 stage with rotary encoders in the x- and y-axes. The microscope and associated components were encased in a climate-controlled environmental chamber built specifically for this purpose. The illumination, filter wheels, focusing, stage movements, and image acquisitions were fully automated and coordinated with publicly available (ImageJ, μManager) software.

Image analysis. Custom ImageJ/Fiji macros and Python scripts[11] were used to identify neurons and draw regions of interest (ROIs) based upon size, morphology, and fluorescence intensity. Additional scripts were

used to identify and draw regions of interest (ROIs) surrounding each cell, and measure fluorescence intensity within individual ROIs. Boxplots were generated using the ggplot package in R, and statistical comparisons accomplished using one-way ANOVA with Tukey's test. Time of death was indicated by disruption of neuronal processes, rounding of the soma or loss of fluorescence intensity[9]. With this information, neuronal survival was assessed using the survival package in R, and differences in survival among neuronal populations determined by Cox proportional hazards analysis. To identify nuclear puncta, we measured the nuclear coefficient of variability (nCV) using code described previously[11–13] that first draws ROIs around each neuron, then draws a second ROI around the nucleus defined by a nuclear marker such as Hoechst or the low-intensity diffuse TDP43-EGFP signal. Within this nuclear ROI, the nCV is calculated as the ratio of the standard deviation of EGFP intensity (integrated over the area of the ROI) divided by the mean EGFP intensity within the ROI. The specificity and sensitivity of nCV values were determined by comparison of single-cell nCV values to the ground truth, in this case puncta determination by visual inspection of individual cells. Receiver-operator characteristic (ROC) curves were plotted as before[11,12], and a threshold was chosen based on maximal specificity to minimize false positives. This threshold was applied to all neurons to predict TDP43-EGFP puncta formation, and percentages calculated on a per-well basis.

Drosophila genetics. Flies were raised at 23°C on standard cornmeal medium with a 12/12-hrs light dark cycle, 60-80% relative humidity. The following fly stocks obtained from Bloomington Drosophila Stock Center (Bloomington, IN) were used in this study: w[1118]; P{w[+mC]=UAS-TDP-43.YFP}8S (BDSC #79589, called TDP-43OE), w[*]; P{w[+mW.hs]=GawB}D42 (BDSC #8816, called D42 Gal4), and w[1118] (BDSC #5905, called w1118). Transgenic expressing human TDP-43 fly (PMID: 20740007) was crossed to D42 Gal4 fly to drive its expression in motor neurons. For genetic control, w1118 (the parental strain used in the generation of TDP-43 transgenic line) was crossed to TDP-43OE. A mixture of both male and female adults was used throughout.

Climbing assay. Fly crosses were made in an egg-laying cage with a removable egg-laying dish. The egg laying dish consisted of a 60x15 mm petri dish containing sucrose agar medium spotted with a fresh dab of yeast paste. Flies were allowed to lay eggs for 24 hours at room temperature. Eggs were collected using a fine paintbrush dampened with water and gentle brushing of the plate to dislodge eggs from the agar. Eggs were then transferred to cornmeal food vials containing either Dimethyl sulfoxide (DMSO 0.05%) solvent or nTRD022 (50 μM). After eclosion, the adult flies were transferred to a fresh supplemented cornmeal food vial. Climbing assay experiments were performed as described in PMID: 26132637. On the day of the experiment, flies were transferred from a single vial into a 250-mL glass graduated cylinder that was sealed with a wax film to prevent escape. Flies were tapped down to the bottom of the cylinder and their climbing behavior was captured using a video camera (Samsung HMX-F90 HD) for 2 min. The number of flies crossing the height of 17.5 cm (190 mL graduation) was manually scored. To avoid variation due to circadian rhythms experiments (for both genotypes) were conducted at the same time of day and in ambient light.

Synthesis of nTRD022

General Experimental Conditions Reactions in anhydrous solvents were carried out in glassware that was flame-dried or oven-dried. Unless noted, reactions were magnetically stirred and conducted under an atmosphere. Air-sensitive reagents and solutions were transferred via syringe and were introduced to the reaction vessel through rubber septa. Solids were introduced under a positive pressure of Ar. Temperatures, other than room temperature (rt); refer to bath temperatures unless otherwise indicated. All commercially obtained solvents and reagents were used as received. ^{1}H and ^{13}C NMR spectra were recorded on Bruker Advance 400. Chemical shifts in ^{1}H NMR spectra are reported in parts per million (ppm) relative to residual chloroform (7.26 ppm) or dimethyl sulfoxide (2.50 ppm) as internal standards. 1H NMR data are reported as follows: chemical shift, multiplicity (s = singlet, d = doublet, m = multiplet), coupling constant in Hertz (Hz) and hydrogen numbers based on integration intensities. ^{13}C NMR chemical shifts are reported in ppm relative to the central peak of $CDCl_3$ (77.16 ppm) or $(CD_3)_2SO$ (39.52 ppm) as internal standards. High resolution mass spectra (LRMS) were obtained using an Agilent 1200 Series Rapid Resolution LC/MS. The purity of the compounds that were tested in the assay was >95% based on ^{1}H.

Synthesis route of nTRD022

Scheme 1. Synthesis of 5-((3-(trifluoromethyl)phenoxy)methyl)isoxazole-3-carboxylic acid

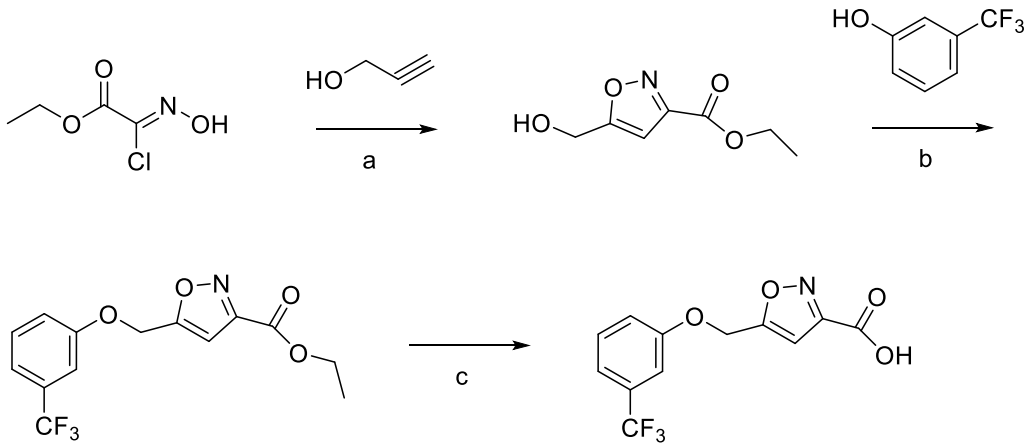

(a) pH 4.0, ACE/H_2O, 15 h; (b) PPh_3,DEAD,THF, 24h; (c) LiOH, H_2O, EtOH, 16 h.

Intermediate ethyl 5-(hydroxymethyl)isoxazole-3-carboxylate:Ethyl (Z)-2-chloro-2-(hydroxyimino)acetate (12 mmol) and prop-2-yn-1-ol (10 mmol) were dissolved in acetone (5 mL, in a round bottom flask). The mixture was stirred at room temperature and was stepwise added 100 mL of 0.1 M phosphate buffer for 15h. Then the mixture was extracted with EtOAc (15mL) for 3 times. Organic extracts were combined, dried with Na_2SO_4, and evaporated under reduced pressure to obtain a crude product. The product was purified by silica gel column chromatography using hexane/ethyl acetate as eluents to give light yellow oil (1.01 g yield: 61.7%).

Intermediate ethyl 5-((3-(trifluoromethyl)phenoxy)methyl)isoxazole-3-carboxylate: The solution obtained by adding ethyl 5-(hydroxymethyl)isoxazole-3-carboxylate (6.4 mmol) and 3-

(trifluoromethyl)phenol (12.8 mmol) to dehydrated THF at 0°C. Triphenylphosphine (12.8 mmol), triethylamine (12.8 mmol) and DIED (9.6mmol) were added to solution under nitrogen protection. The reaction mixture was warmed to room temperature and stirred for 2 hours, then poured into water, and the mixture was extracted twice with ethyl acetate. The organic layer was washed with saturated aqueous brine, dried over Na_2SO_4 and then concentrated under pressure. The product was purified by silica gel column chromatography using hexane/ethyl acetate as eluents to give light white solid (1.56 g yield: 77.4%).

Intermediate 5-((3-(trifluoromethyl)phenoxy)methyl)isoxazole-3-carboxylic acid: Ethyl 5-((3-(trifluoromethyl)phenoxy)methyl)isoxazole-3-carboxylate (5 mmol) was added to ethanol (15 mL), and LiOH (15 mmol) and H_2O (6.5 mL) were further added thereto. The mixture was stirred at room temperature for 16 hours and then concentrated under reduced pressure. Dilute hydrochloric acid was added to the concentrate, the mixture was cooled to 0 ° C, and the precipitated solid was filtered. The resulting solid was dried under reduced pressure to give 1.11 g of product (yield: 75.1%).

Scheme 2. Synthesis of 1-(2-aminoethyl)piperidin-3-ol

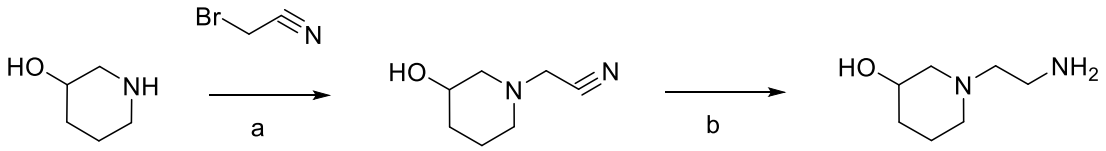

(a) Et_3N, THF, 0.5h; (b) PPh_3,DEAD,THF, 24h.

Intermediate 2-(3-hydroxypiperidin-1-yl)acetonitrile: Bromoacetonitrile (10 mmol) was added dropwise to a solution of 3-hydroxypiperidine (10 mmol) in dry THF (25 mL) under N_2, while the temperature was maintained between 45 and 50 °C. Following addition of Bromoacetonitrile, the solution was refluxed for 30 min, before allowing the solution to cool to room temperature. The solvent was removed in vacuo and the residual oil was purified by flash chromatography using CH_2Cl_2/CH3OH as eluent. The title compound was obtained as a straw-colored oil (79.6mg yield:56.9%).

Intermediate 1-(2-aminoethyl)piperidin-3-ol: $LiAlH_4$ (20 mmol) was added to dry THF (20 mL) at 0 °C in a three-neck round bottom flask under N_2. The solution was stirred for 15 min before the 3-hydroxypiperidin-1-ylacetonitrile (5 mmol), diluted in dry THF (5 mL), was added slowly via syringe. The reaction mixture was then refluxed for 5 h before allowing the solution to cool to room temperature. Excess $LiAlH_4$ was destroyed by dropwise addition of 2.4 mL of H_2O and 2.4 mL of NaOH (15%), and finally EtOAc was added dropwise until no effervesence was observed. The formed granular precipitate (lithium hydroxide and aluminum hydroxide) was filtered off and washed several times with CH_2Cl_2 and EtOAc. The organic layer was dried ($MgSO_4$) and the solvent was removed in vacuo to yield a thick yellowish oil. the residual oil was directly used in next step without purification (52.6mg yield:64.4%).

Scheme 3. Synthesis of nTRD022

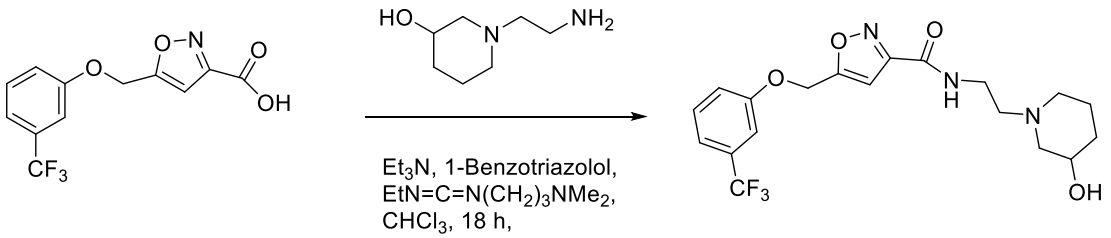

Synthesis of nTRD022: 5-((3-(trifluoromethyl)phenoxy)methyl)isoxazole-3-carboxylic acid (0.4 mmol), 1-(2-aminoethyl)piperidin-3-ol(0.5 mmol) , triethylamine (0.5 mmol) and 1-hydroxybenzotriazole (0.05 mmol) were added to chloroform (2 mL). 1-Ethyl-3-(3-dimethylaminopropyl) carbodiimide hydrochloride (0.5 mmol) was added to the mixture at room temperature, and the mixture was stirred overnight and then concentrated under reduced pressure. Dilute hydrochloric acid was added to the concentrate, and the mixture was extracted twice with ethyl acetate. The organic layer was washed with saturated saline water, dried over anhydrous sodium sulfate, and then concentrated under reduced pressure. The residue was applied to a silica gel column chromatography to obtain nTRD022 (90.8 mg, yield: 57.1%). ^{1}H NMR (400 MHz, Chloroform-d) δ 7.46 – 7.36 (m, 1H), 7.26 (ddt, J = 7.7, 1.6, 0.8 Hz, 1H), 7.17 (t, J = 2.1 Hz, 1H), 7.13 – 7.07 (m, 1H), 6.78 (s, 1H), 5.20 (d, J = 0.8 Hz, 2H), 3.81 (dp, J = 6.3, 3.2 Hz, 1H), 3.51 (p, J = 5.7 Hz, 2H), 2.56 (t, J = 6.1 Hz, 4H), 2.40 (d, J = 27.8 Hz, 5H), 1.85 – 1.74 (m, 2H), 1.71 – 1.61 (m, 1H), 1.58 – 1.47 (m, 2H). HRMS (EI) m/z [M + H]+ calculated for $C_{19}H_{22}F_3N_3O_4$: 414.16352, found 414.16351.

Spectral Data

^{1}H NMR of nTRD022

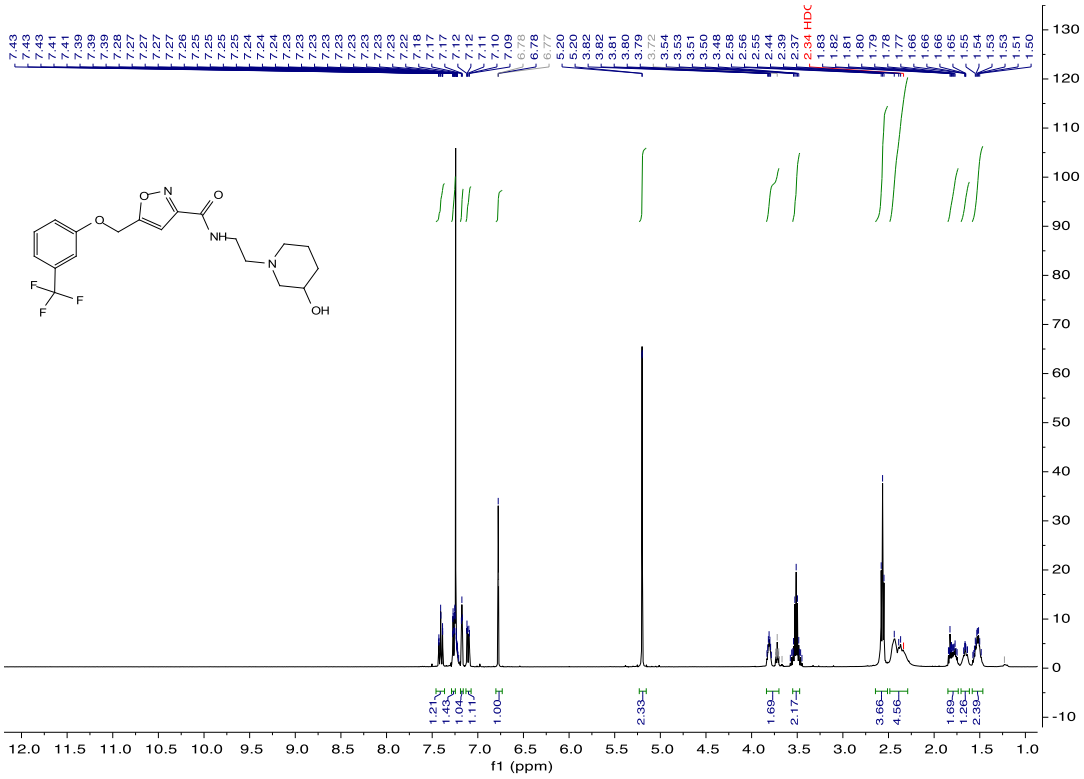

^{13}C NMR of nTRD022

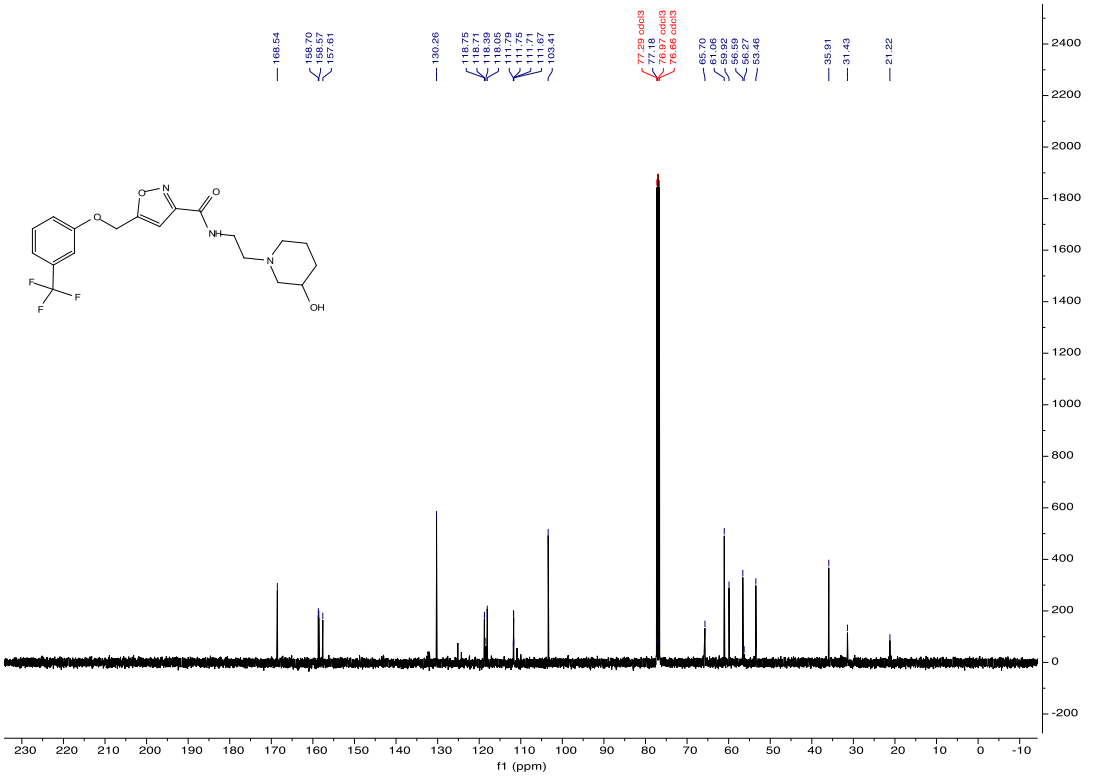

HRMS of nTRD022

Generic Display Report

Analysis Info

Analysis Name	D:\Data\Krishna\2019\ESI\04-April_2019-ESI\2494149_YD-80R_000001.d	Acquisition Date	4/26/2019 8:35:51 AM
Method	150-3000	Operator	
Sample Name	2494149_YD-80R	Instrument	solariX XR
Comment	dissolved in 400 ul ACN/H2O, then dissolved 62500x in ACN/H2O/0.1%FA		

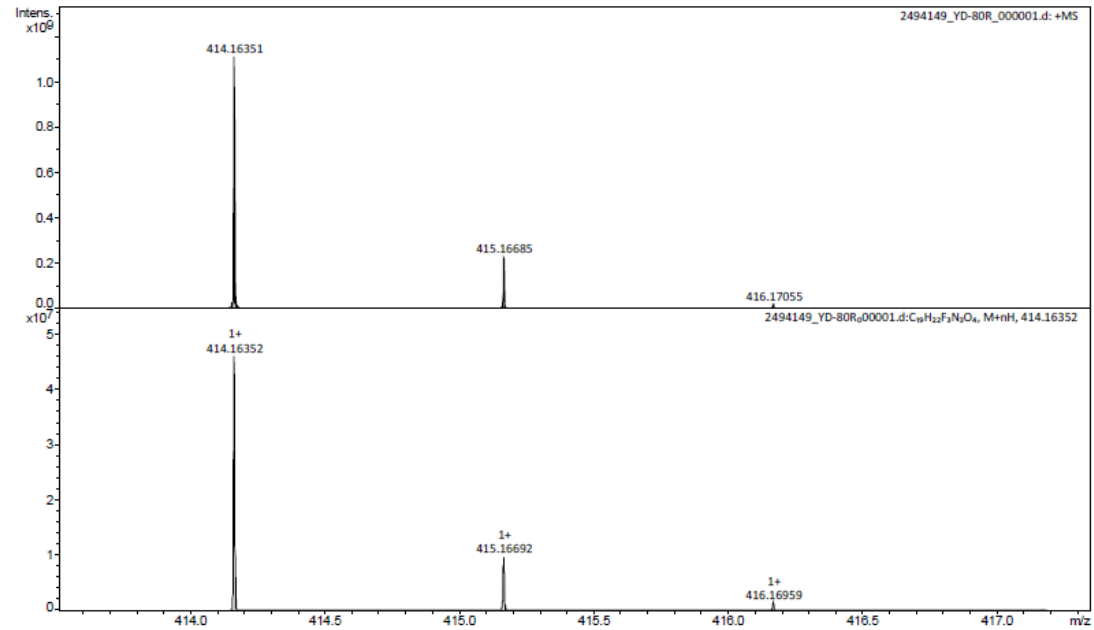

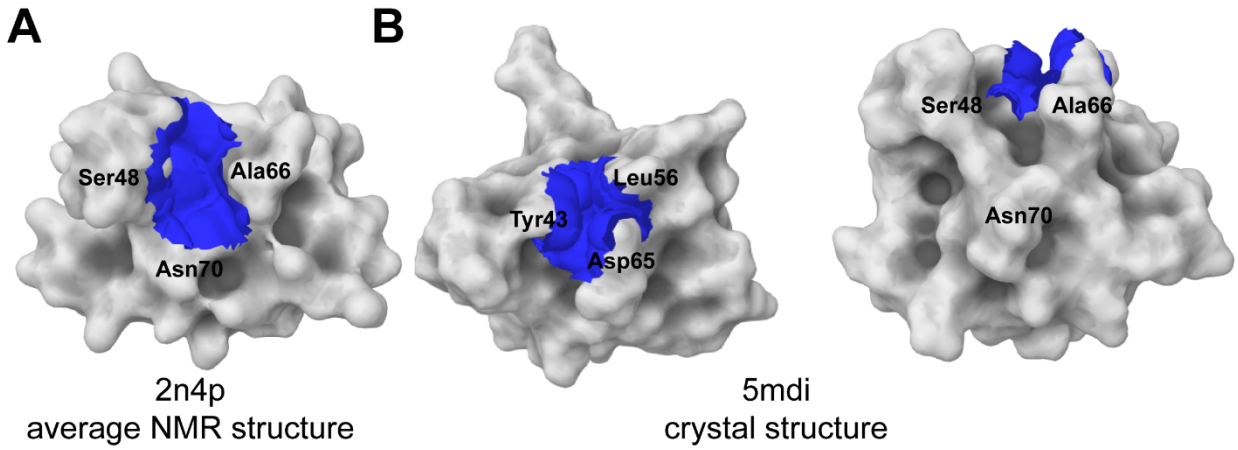

Figure S1: Sitemap of TDP-43 NTD structures. Surface representation of docking pockets (*blue*) found using SiteMap on the (**A**) average NMR structure (PDB ID: 2n4p[14]) or (**B**) crystal structure (PDB ID: 5mdi[4]).

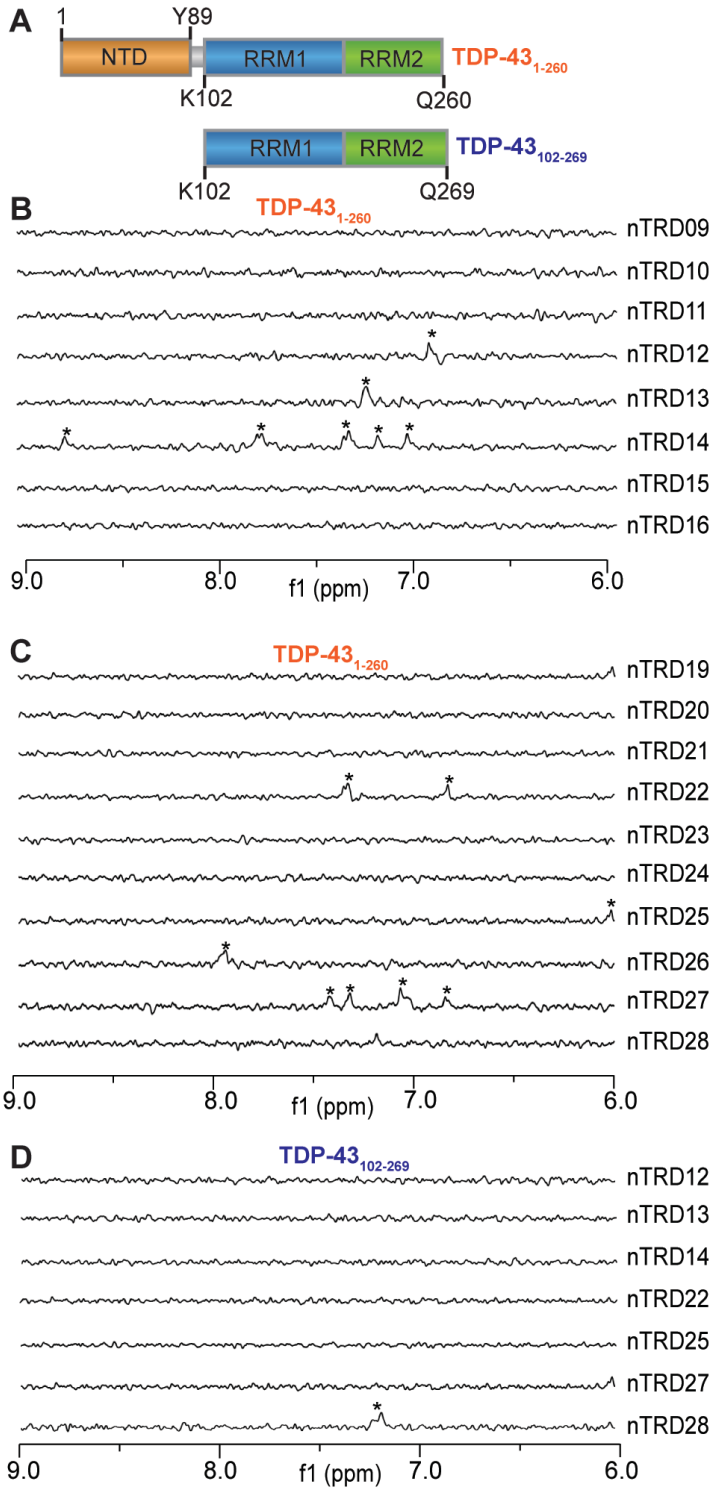

Supplementary Figure 2. STD-NMR screening for compounds. **A.** Two different constructs were used for STD-NMR screening. 1D ^{1}H STD-NMR showing on-resonance difference spectrum of 500 μM of compounds nTRD09–16 (**B**) or nTRD19–28 (**C**) with 5 μM TDP43$_{1\text{-}260}$. **D.** Positive hits from the first round of STD-NMR screening were tested against TDP43$_{102\text{-}269}$ in the same conditions. Asterisks indicate positive signal.

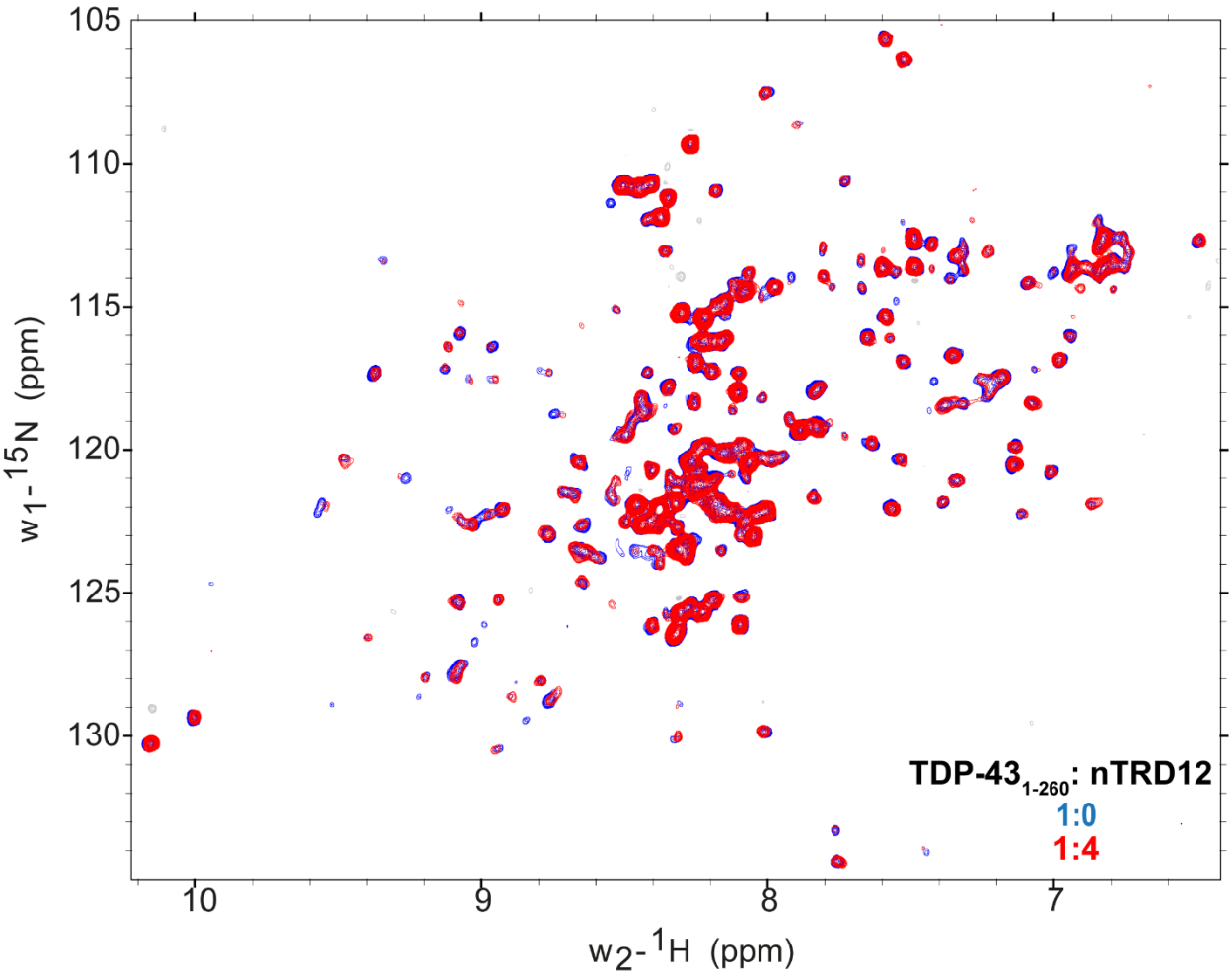
105
110
115
120
125
130
w_1-^{15}N (ppm)
10
9
8
7
w_2-^{1}H (ppm)
TDP-43$_{1-260}$: nTRD12
1:0
1:4

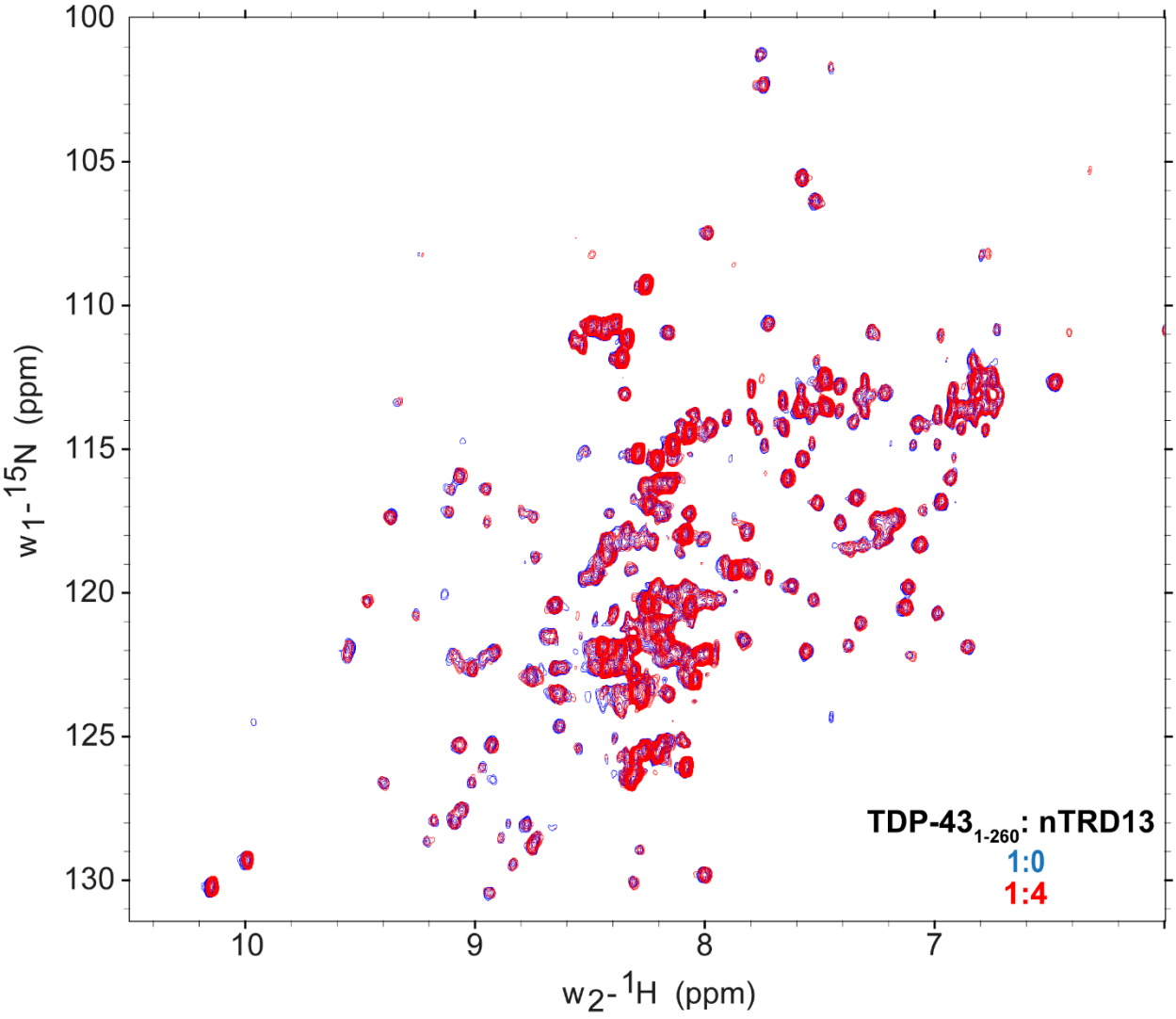
100
105
110
115
120
125
130
w_1-^{15}N (ppm)
10
9
8
7
w_2-^{1}H (ppm)
TDP-43$_{1-260}$: nTRD13
1:0
1:4

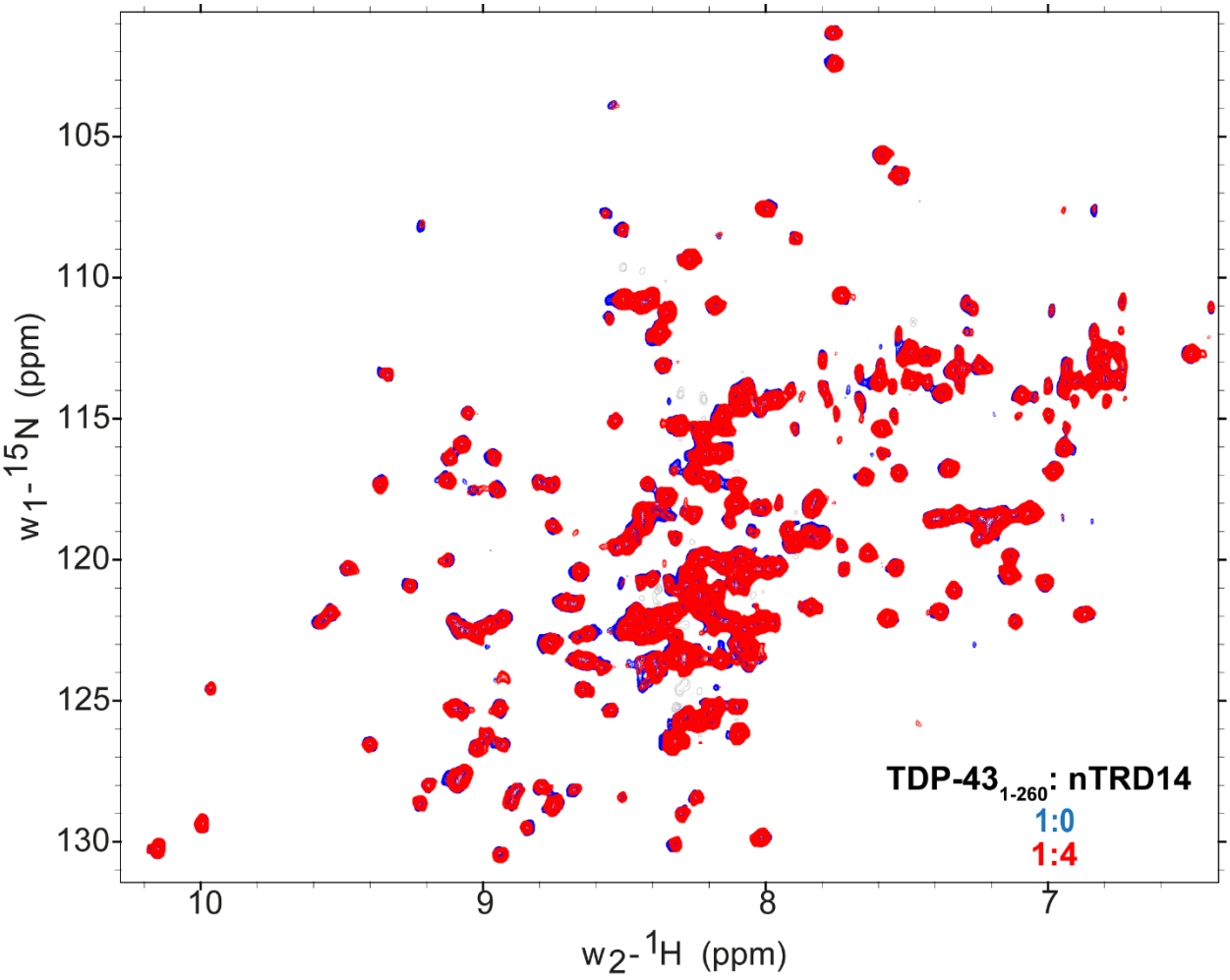
105
110
115
120
125
130
w_1-^{15}N (ppm)
10
9
8
7
w_2-^{1}H (ppm)
TDP-43$_{1-260}$: nTRD14
1:0
1:4

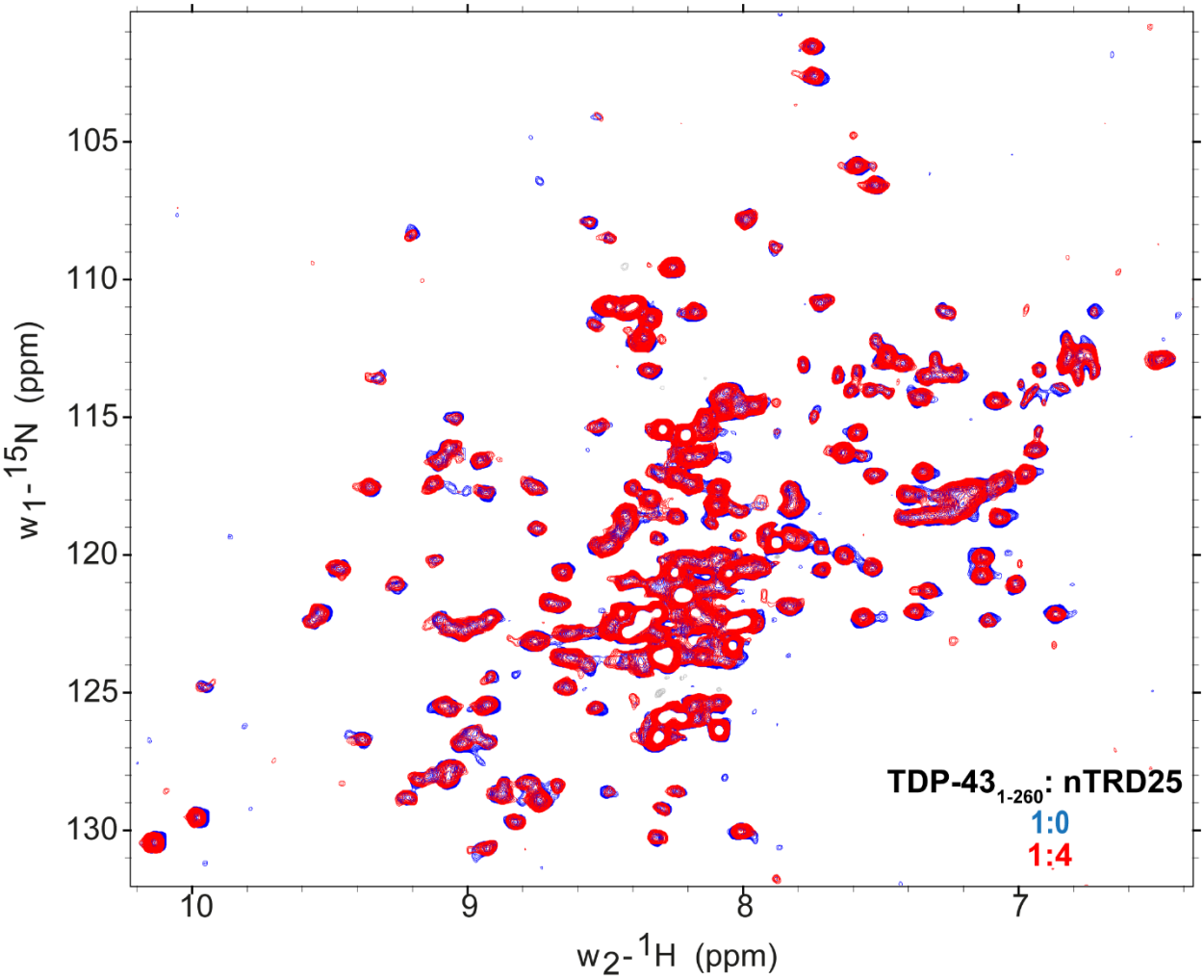
105
110
115
120
125
130
w1-15N (ppm)
10
9
8
7
w2-1H (ppm)
TDP-431-260: nTRD25
1:0
1:4

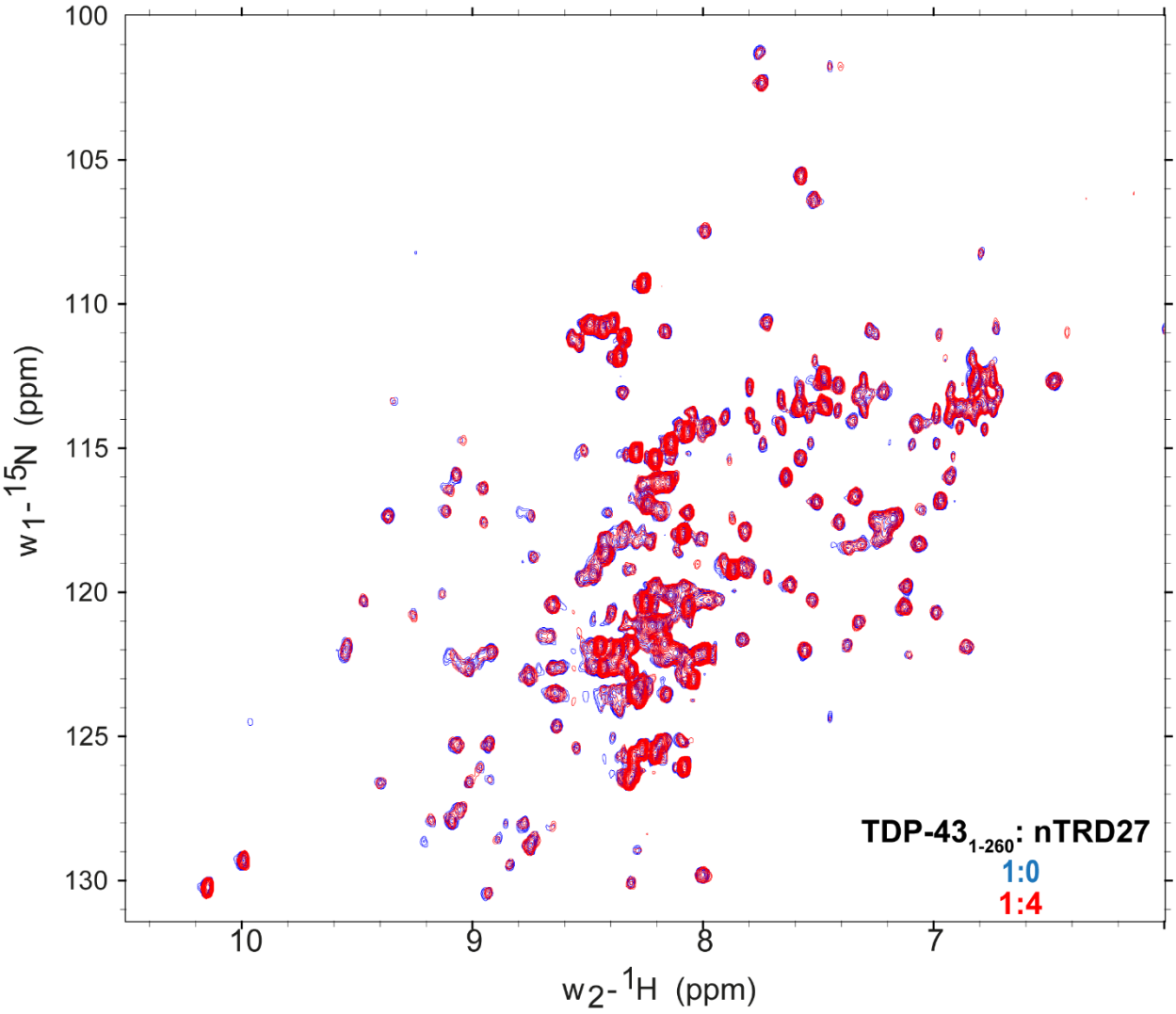
100
105
110
115
120
125
130
w1- 15N (ppm)
10
9
8
7
w2- 1H (ppm)
TDP-431-260: nTRD27
1:0
1:4

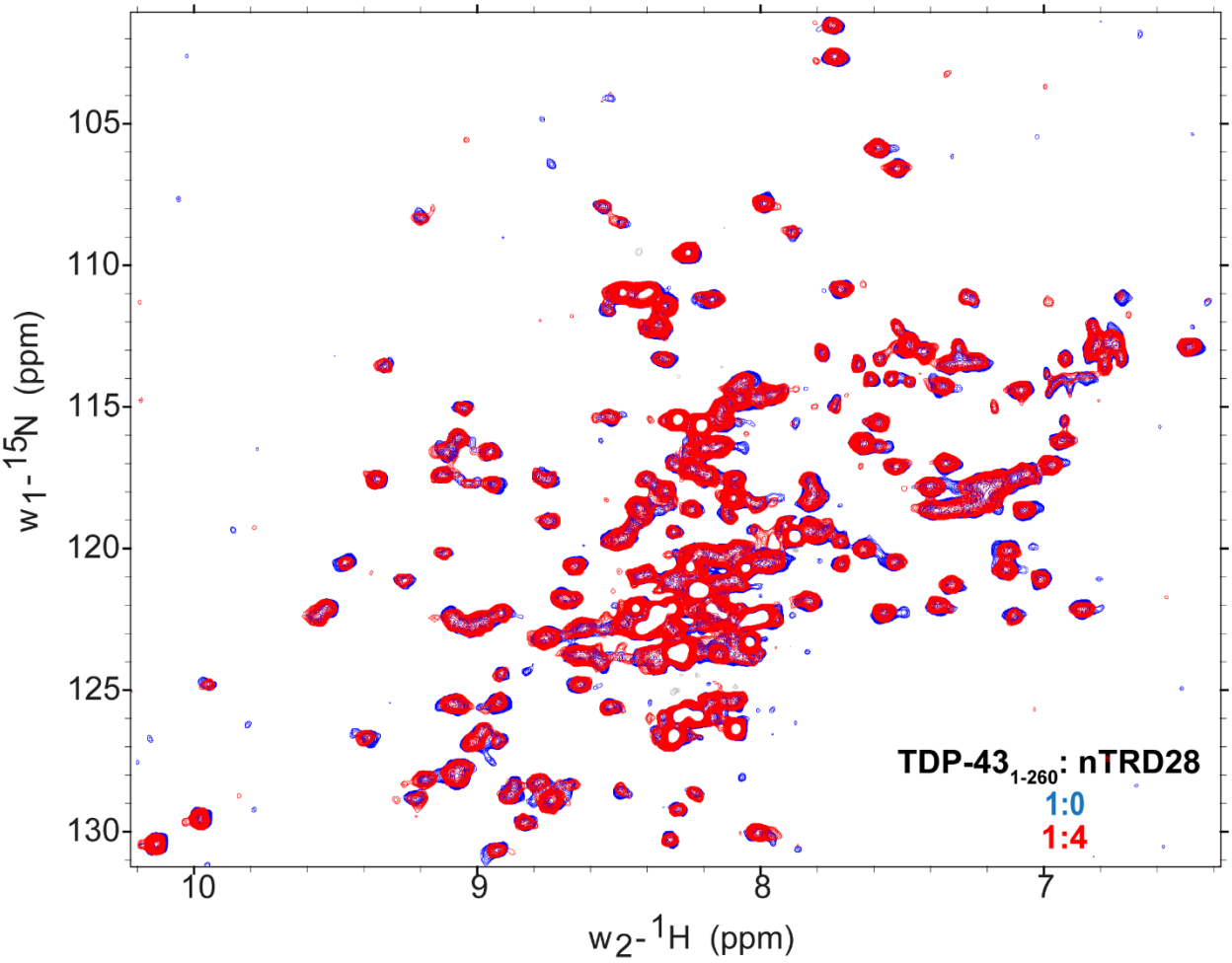

Supplementary Figure 3: Superposition of ^{1}H-^{15}N heteronuclear single quantum correlation spectroscopy (HSQC) spectra of ^{15}N-labeled human TDP43$_{1\text{-}260}$ (100 µM), with DMSO (*blue*) and in complex with positive nTRD binders (400 µM) in *red.*

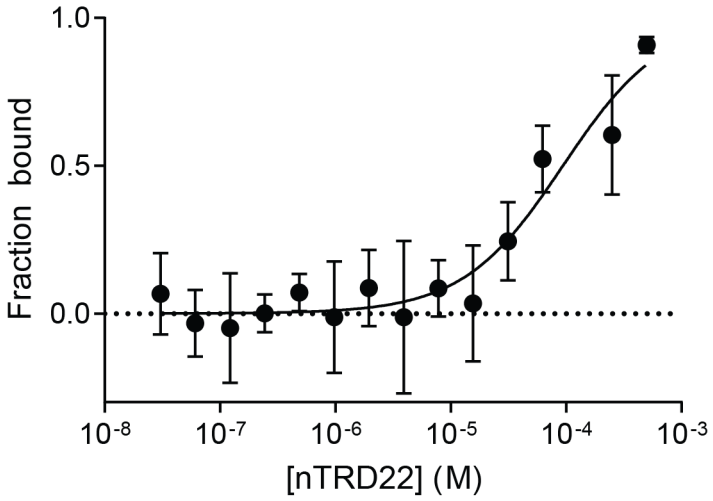

Supplementary Figure 4: MST values from thermographs of NT-647 labeled $TDP43_{1-102}$ in presence of increasing concentrations (0.03 μM – 1 mM) of nTRD22 were used to determine dissociation constant for binding of nTRD22 to $TDP43_{1-102}$. Apparent Kd of 96±36 μM. Data is presented as mean ± SD (n = 3).

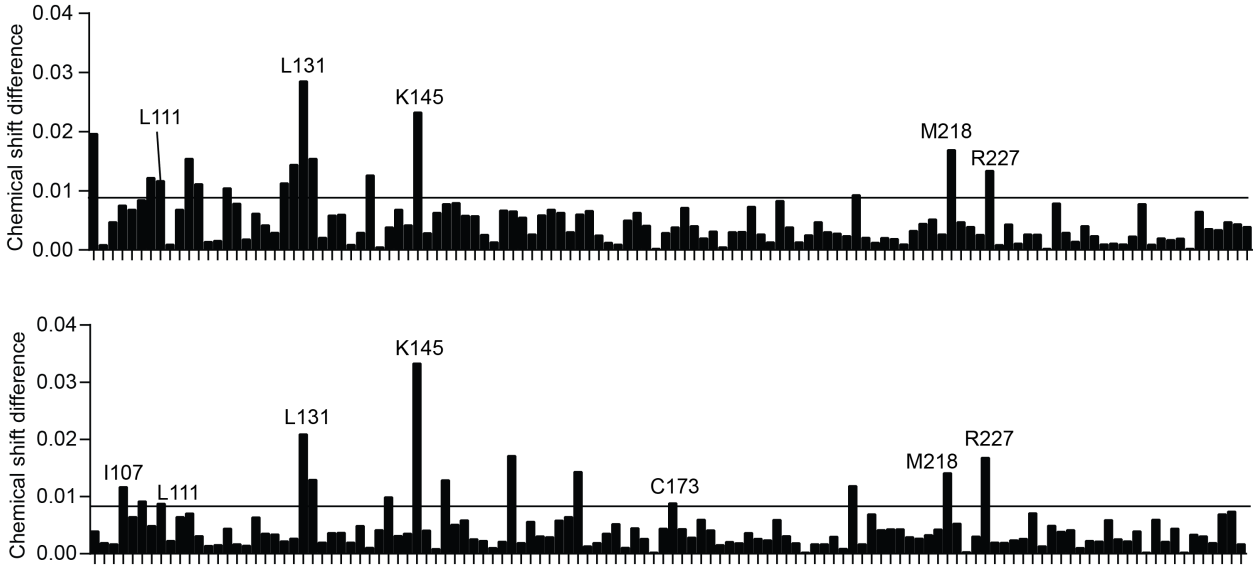

Supplementary Figure 5: Chemical shift changes for assigned residues of the ^{15}N-labeled TDP-43$_{1\text{-}260}$ (RRM portion only) upon complex formation with nTRD22. The chemical shift changes of cross-peaks were calculated as described in the Methods section.

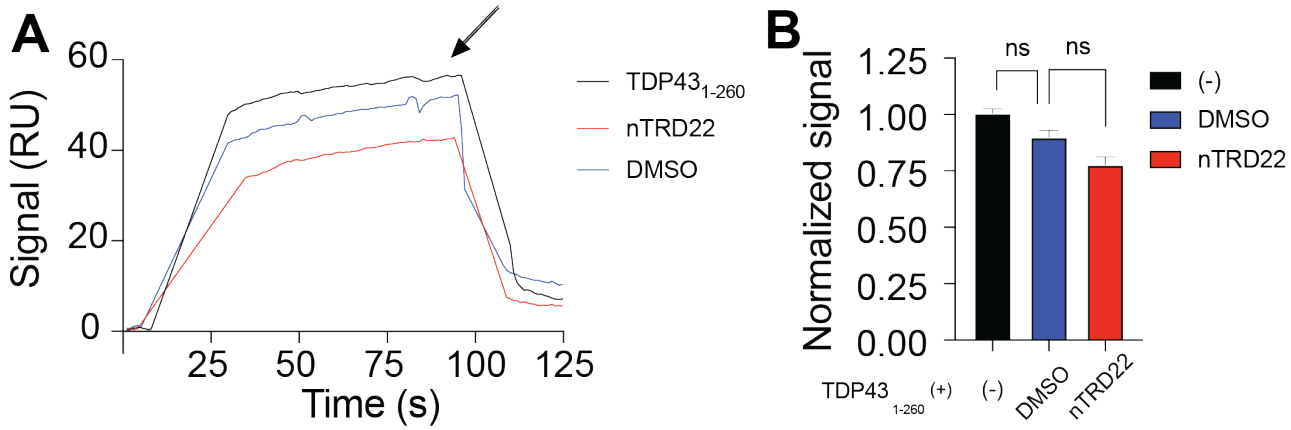

Supplementary Figure 6: nTRD22 does not affect the dimerization of N-terminal domain of TDP-43. **A.** Representative SPR sensograms showing the signal for dimerization of 500 nM TDP-$43_{1\text{-}260}$ and immobilized NTD (TDP-$43_{1\text{-}102}$) in the presence (*red*) or absence (*blue*) of 200 μM nTRD22 dissolved in DMSO.. **B.** Quantification of SPR signals (*arrow* in A.) shows no significant change in the dimerization in the presence of nTRD22 compared to DMSO. Data is presented as mean ± SEM (n =3 replicates for each condition). Statistical difference was assessed by a Kruskal-Wallis test (ns, $p>0.05$).

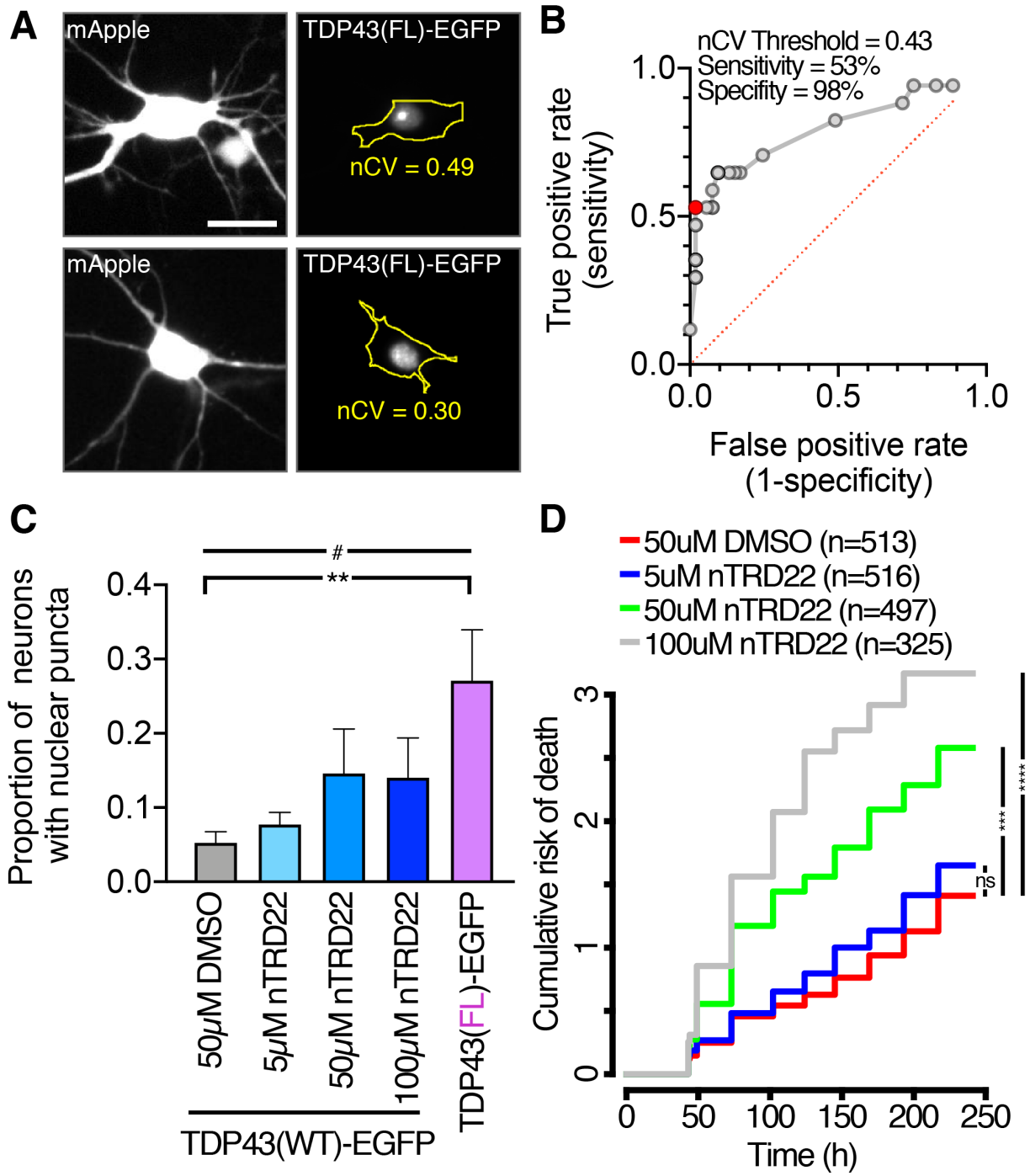

Supplementary Figure 7: Live-cell detection of TDP43-EGFP puncta in response to nTRD22. A. Fluorescence microscopy of neurons expressing the cell marker mApple and an EGFP-labeled TDP43 variant harboring the F147L and F149L mutations [TDP43(FL)-EGFP]. As in previous studies, TDP43(FL)-EGFP forms nuclear puncta in association with its inability to bind RNA[8]. Using the mApple signal as a reference, automated scripts detect neurons and draw a region of interest (ROI, yellow) around the soma. This ROI is used to detect a nuclear coefficient of variation (nCV) for neurons displaying punctate (top) or diffuse (bottom) distributions of TDP43(FL)-EGFP. Scale bar, 25 μm. **B**. Receiver-operator

characteristic (ROC) curve for nCV as a predictor of nuclear TDP43(FL)-EGFP puncta. We selected a threshold of 0.43, corresponding to 53% sensitivity and 98% specificity, to minimize the incidence of false positives. **C**. Automated analysis of neurons expressing TDP43(WT)-EGFP or TDP43(FL)-EGFP treated with DMSO or varying concentrations of nTRD022. Values combined from >20 technical and 3 biological replicates. **p=0.006, one-way ANOVA with Dunnett's post-test; #p=0.001 for linear trend, one-way ANOVA. **D**. Automated survival analysis of neurons treated with vehicle (DMSO) or nTRD22. Data pooled from 24 technical replicates and 3 biological replicates per condition. Differences in the risk of death were determined by Cox proportional hazards analysis, using the DMSO-treated cells as a reference. n = number of neurons; ns, not significant; ***hazard ratio = 2.2, $p<2x10^{-16}$; ****hazard ratio=3.2, $p<2x10^{-16}$.

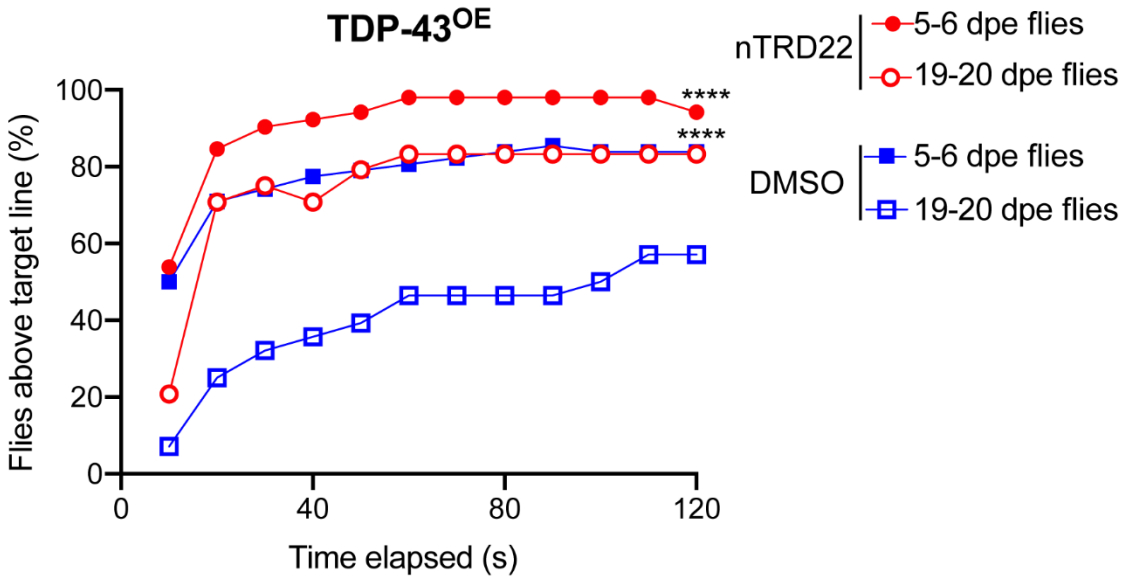

Supplementary Figure 8: Fly food supplemented with nTRD22 (50 μM) resulted in increased motor performance compared to DMSO (0.05%) treated flies in young individuals (5-6 days post eclosion ; dpe) as well as aged individuals (19-20 dpe). (n = 60, **** $p<0.0001$, Two-Way ANOVA).

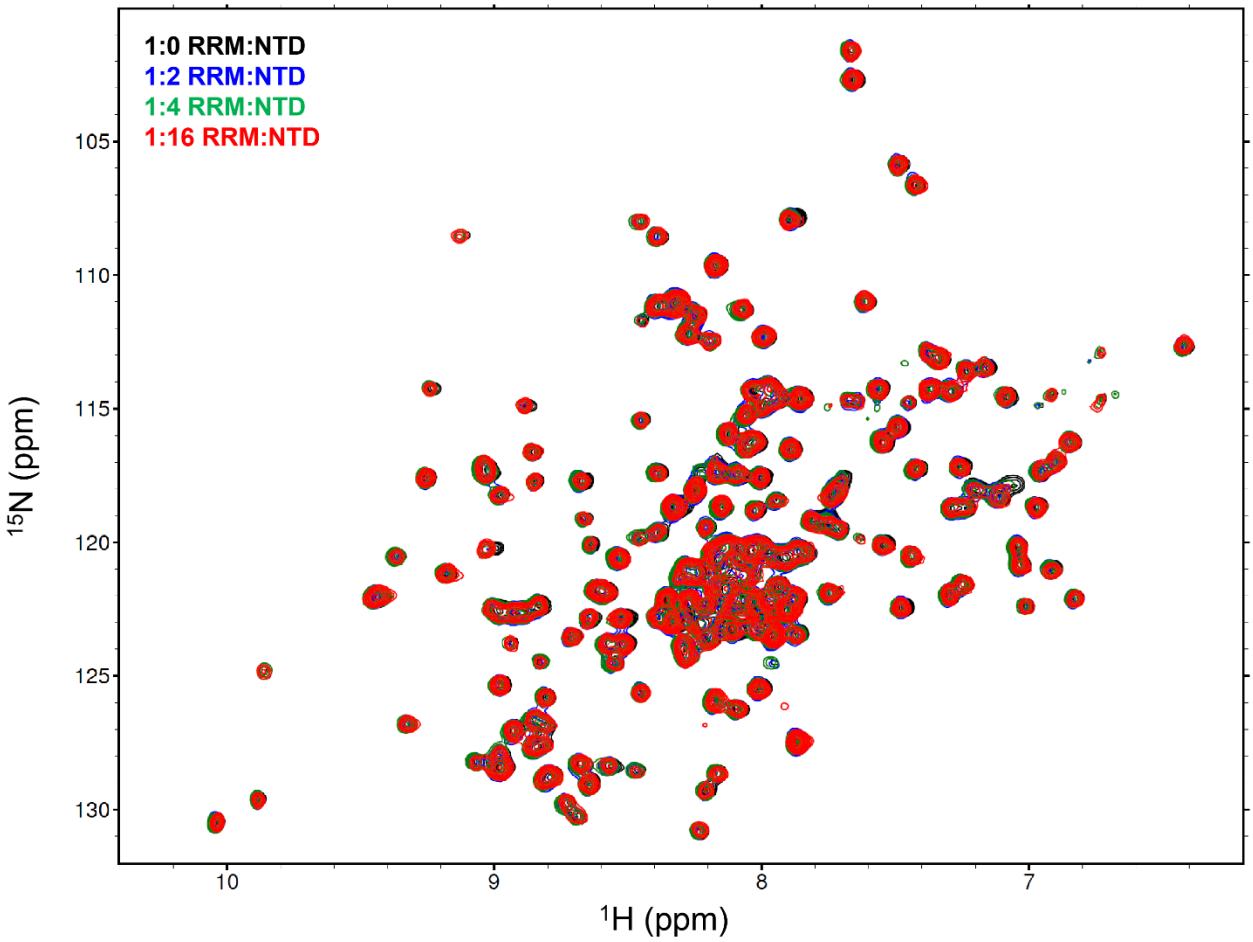

Supplementary Figure 9: Superposition of ^{1}H-^{15}N heteronuclear single quantum correlation spectroscopy (HSQC) spectra of ^{15}N-labeled human TDP43$_{102-269}$ (100 μM), free (*black*) and in complex with TDP43 NTD with different ratios.

REFERENCES

(1) Irwin, J. J., Duan, D., Torosyan, H., Doak, A. K., Ziebart, K. T., Sterling, T., Tumanian, G., and Shoichet, B. K. (2015) An Aggregation Advisor for Ligand Discovery. *J. Med. Chem. 58*, 7076–7087.

(2) Scott, D. D., Francois-Moutal, L., Kumirov, V. K., and Khanna, M. (2019) 1 H, 15 N and 13 C backbone assignment of apo TDP-43 RNA recognition motifs. *Biomol. NMR Assign. 13*, 163–167.

(3) François-Moutal, L., Felemban, R., Scott, D. D., Sayegh, M. R., Miranda, V. G., Perez-Miller, S., Khanna, R., Gokhale, V., Zarnescu, D. C., and Khanna, M. (2019) Small Molecule Targeting TDP-43's RNA Recognition Motifs Reduces Locomotor Defects in a Drosophila Model of Amyotrophic Lateral Sclerosis (ALS). *ACS Chem. Biol. 14*, 2006–2013.

(4) Afroz, T., Hock, E. M., Ernst, P., Foglieni, C., Jambeau, M., Gilhespy, L. A. B., Laferriere, F., Maniecka, Z., Plückthun, A., Mittl, P., Paganetti, P., Allain, F. H. T., and Polymenidou, M. (2017) Functional and dynamic polymerization of the ALS-linked protein TDP-43 antagonizes its pathologic aggregation. *Nat. Commun. 8*.

(5) Mompeán, M., Romano, V., Pantoja-Uceda, D., Stuani, C., Baralle, F. E., Buratti, E., and Laurents, D. V. (2016) The TDP-43 N-terminal domain structure at high resolution. *FEBS J. 283*, 1242–1260.

(6) François-Moutal, L., Jahanbakhsh, S., Nelson, A. D. L., Ray, D., Scott, D. D., Hennefarth, M. R., Moutal, A., Perez-Miller, S., Ambrose, A. J., Al-Shamari, A., Coursodon, P., Meechoovet, B., Reiman, R., Lyons, E., Beilstein, M., Chapman, E., Morris, Q. D., Van Keuren-Jensen, K., Hughes, T. R., Khanna, R., Koehler, C., Jen, J., Gokhale, V., and Khanna, M. (2018) A Chemical Biology Approach to Model Pontocerebellar Hypoplasia Type 1B (PCH1B). *ACS Chem. Biol. 13*, 3000–3010.

(7) Lee, W., Tonelli, M., and Markley, J. L. (2015) NMRFAM-SPARKY: Enhanced software for biomolecular NMR spectroscopy. *Bioinformatics 31*, 1325–1327.

(8) Flores, B. N., Li, X., Malik, A. M., Martinez, J., Beg, A. A., and Barmada, S. J. (2019) An Intramolecular Salt Bridge Linking TDP43 RNA Binding, Protein Stability, and TDP43-Dependent Neurodegeneration. *Cell Rep. 27*, 1133-1150.e8.

(9) Weskamp, K., Safren, N., Miguez, R., and Barmada, S. (2019) Monitoring neuronal survival via longitudinal fluorescence microscopy. *J. Vis. Exp.*

(10) Malik, A. M., Miguez, R. A., Li, X., Ho, Y. S., Feldman, E. L., and Barmada, S. J. (2018) Matrin 3-dependent neurotoxicity is modified by nucleic acid binding and nucleocytoplasmic localization. *Elife 7*.

(11) Malik, A. M., Miguez, R. A., Li, X., Ho, Y. S., Feldman, E. L., and Barmada, S. J. (2018) Matrin 3-dependent neurotoxicity is modified by nucleic acid binding and nucleocytoplasmic localization. *Elife*.

(12) Sharkey, L. M., Safren, N., Pithadia, A. S., Gerson, J. E., Dulchavsky, M., Fischer, S., Patel, R., Lantis, G., Ashraf, N., Kim, J. H., Meliki, A., Minakawa, E. N., Barmada, S. J., Ivanova, M. I., and Paulson, H. L. (2018) Mutant UBQLN2 promotes toxicity by modulating intrinsic self-assembly. *Proc. Natl. Acad. Sci. U. S. A.*

(13) Archbold, H. C., Jackson, K. L., Arora, A., Weskamp, K., Tank, E. M. H., Li, X., Miguez, R., Dayton, R. D., Tamir, S., Klein, R. L., and Barmada, S. J. (2018) TDP43 nuclear export and neurodegeneration in models of amyotrophic lateral sclerosis and frontotemporal dementia. *Sci. Rep. 8*.

(14) Mompeán, M., Romano, V., Pantoja-Uceda, D., Stuani, C., Baralle, F. E., Buratti, E., and Laurents, D. V. (2016) The TDP-43 N-terminal domain structure at high resolution. *FEBS J. 283*, 1242–1260.